Experiments and Simulations of Ion-Enhanced Interfacial Chemistry on Aqueous NaCl Aerosols

E. M. Knipping, M. J. Lakin, K. L. Foster, P. Jungwirth, D. J. Tobias, R. B. Gerber, D. Dabdub, B. J. Finlayson-Pitts R.

A combination of experimental, molecular dynamics, and kinetics modeling studies is applied to a system of concentrated aqueous sodium chloride particles suspended in air at room temperature with ozone, irradiated at 254 nanometers to generate hydroxyl radicals. Measurements of the observed gaseous molecular chlorine product are explainable only if reactions at the air-water interface are dominant. Molecular dynamics simulations show the availability of substantial amounts of chloride ions for reaction at the interface, and quantum chemical calculations predict that in the gas phase chloride ions will strongly attract hydroxl radicals. Model extrapolation to the marine boundary layer yields daytime chlorine atom concentrations that are in good agreement with estimates based on field measurements of the decay of selected organics over the Southern Ocean and the North Atlantic. Thus, ion-enhanced interactions with gases at aqueous interfaces may play a more generalized and important role in the chemistry of concentrated inorganic salt solutions than was previously recognized.

Processes at the air-water interface may play a key role in the uptake and reactions of gases with liquid particles in the troposphere. For example, SO_2 has been shown to form a unique bound complex at the interface that participates in its oxidation to sulfate (I–3). Similarly, reactions between gases such as Cl_2 and O_3 and inorganic ions such as Br^- and I^- in solution have been shown to occur not only in the bulk liquid but also at the interface, leading to enhanced uptake and/or reactions of the gases (4–6).

Zetzsch and co-workers (7) report that an unidentified chlorine atom precursor is generated upon irradiation of seawater aerosol with simulated sunlight in the presence of ozone. Subsequently, our laboratory has shown that gaseous $\operatorname{Cl}_2(8)$ is generated from deliquesced sea salt particles in the presence of O_3 and 254-nm radiation. Photolysis of O_3 generates OH radicals in the gas phase, which can be taken up into the particles

$$O_3 + hv \rightarrow O(^1D) + O_2$$
 (1)

$$O(^{1}D) + M \rightarrow O(^{3}P)$$
 (2)

$$O(^{1}D) + H_{2}O \rightarrow 2OH_{(g)}$$
 (3)

$$OH_{(g)} \rightarrow OH_{(aq)}$$
 (4)

where h ν is light of wavelength 254 nm, $O(^1D)$ is an electronically excited oxygen atom, g indicates gaseous, and aq indicates aqueous. OH is known to react in solution with Cl^- , ultimately generating Cl_2

$$OH_{(aq)} + Cl^- \leftrightarrow HOCl^-$$
 (5)

$$HOCl^- + H^+ \rightarrow H_2O + Cl$$
 (6

$$Cl + Cl^{-} \rightarrow Cl_{2}^{-} \tag{7}$$

$$2Cl_2^- \rightarrow Cl_{2(aq)} + 2Cl^- \tag{8}$$

$$Cl_{2(aq)} \rightarrow Cl_{2(g)}$$
 (9)

These reactions are dominant for Cl_2 production under the chamber conditions. However, a variety of additional reactions can also contribute, such as $\text{HOCl} + \text{Cl}^- + \text{H}^+ \rightarrow \text{Cl}_2 + \text{H}_2\text{O}$, which dominates under atmospheric conditions. Such bulk aqueous-phase chemistry is included in current models of sea salt reactions in the marine boundary layer (9, 10).

Because of the complex composition of sea salt (11), constituents such as various trace metals have the potential for catalysis. Here we studied reactions of NaCl alone in order to simplify the potential chemistry. A comprehensive computational chemical kinetics model, which incorporates the known gas- and aqueous-phase chemistry in the particles as well as the mass transfer processes, is used to explore quantitatively the chemistry of this simplified system. We show that experimental results and model predictions

can only be reconciled if reactions of gases with ions at the interface control the chemistry. Molecular dynamics simulations of NaCl dissolved in water clusters and quantum chemical calculations support this mechanism. Moreover, they suggest that strong interactions of gases with ions at the interface of concentrated solutions are probably a general property of atmospheric aerosol particles and should be taken into account in understanding and modeling atmospheric processes.

Aerosol chamber studies of the O3-NaCl photochemical system. Dry NaCl particles in air were placed in a chamber described in detail elsewhere (12) and the relative humidity (RH) was increased above the deliquescence point (75% RH) to form concentrated salt solutions. At a RH of 82% and temperature of 297 K, typical of these experiments, the particles are concentrated salt solutions with a concentration of 20 weight percent (wt. %) (13). Ozone was added, but no production of Cl2 was observed until the mixture was irradiated at 254 nm, generating OH via reactions 1 through 4. After the addition of ozone, differential optical absorption spectroscopy was used to follow O₃, other gas-phase species such as CO2 were measured with Fourier-transform infrared spectroscopy (FTIR), and Cl2 was measured by atmospheric pressure ionization-mass spectrometry (API-MS).

Figure 1 shows Cl₂ production in three experiments at different initial ozone concentrations. The Cl₂ production is similar to that observed from sea salt particles (8), showing that the minor components are not important in this reaction. Although the initial ozone concentration decreases by a factor of about 6, the rate of initial Cl₂ production decreases by a factor of less than 2 and the peak Cl₂ concentrations by a factor of less than 4. Indeed, the initial rate of Cl2 production appears to follow primarily the particle surface area and volume (which tend to change to a similar extent simultaneously in these experiments). This is expected if a key step in the Cl₂ production is the reaction of OH with Cl⁻, because modeled OH concentrations for the gas-phase reactions in this system are relatively insensitive to the initial O₃ concentration.

Computational kinetic model studies. To evaluate mechanisms of production of Cl_2 in this system with known gas- and bulk aqueousphase chemistry, we used a computer kinetic model (14). The model, MAGIC (Model of Aerosol, Gas and Interfacial Chemistry), includes 17 gas-phase species (Table 1) undergoing 52 reactions, combined with 32 aqueousphase species undergoing 99 reactions, including reactions 1 through 9. Mass transfer of species between the gas and aqueous phase (15) is treated with the method of Schwartz (16). Namely, the temporal variations of the concentrations of the gas-phase species, $C_{\rm g}$, and the aqueous phase species, $C_{\rm aq}$, are described by a

¹Department of Mechanical and Aerospace Engineering, ²Department of Chemistry, University of California, Irvine, Irvine, CA 92697, USA. ³J. Heyrovsky Institute of Physical Chemistry, Academy of Sciences of the Czech Republic, Dolejškova 3, 18223, Prague 8, Czech Republic. ⁴Department of Physical Chemistry and the Fritz Haber Research Center, The Hebrew University of Jerusalem, Jerusalem 91904, Israel.

^{*}To whom correspondence should be addressed. E-mail: bjfinlay@uci.edu

system of coupled differential equations of the form

$$\frac{dC_{g}}{dt} = -k_{mt}w_{L}C_{g} + \frac{k_{mt}}{H_{A}RT}C_{aq}w_{L} + R_{g}$$
(10)

$$\frac{dC_{\rm aq}}{dt} = k_{\rm mt}C_{\rm g} - \frac{k_{\rm mt}}{H_{\rm A}RT} C_{\rm aq} + \langle R_{\rm aq} \rangle \quad (11)$$

where $k_{\rm mt}$ is the mass transfer coefficient, $w_{\rm L}$ is the dimensionless volumetric liquid water mix-

ing ratio, $H_{\rm A}$ is the Henry's Law coefficient, R is the universal gas constant, T is the chamber temperature, $\langle R_{\rm aq} \rangle$ is the spatially averaged bulk aqueous-phase reaction rate, and $R_{\rm g}$ is the gasphase reaction rate. Because of the high ionic strengths encountered in the droplets, the reactivity of the species in the aqueous phase is described by their activities. Activity coefficients are calculated explicitly for the species ${\rm H^+}, {\rm Na^+}, {\rm Cl^-}, {\rm ClO_3^-}, {\rm OH^-}, {\rm CO_2}, {\rm and O_2}$ with

the Pitzer ion interaction approach (17). For other species, the Guntelberg approximation of the Debye-Hückel limiting law is used (18). An additional term, $R_{\rm int}$, is added to Eqs. 10 and 11 to account for interfacial reactions.

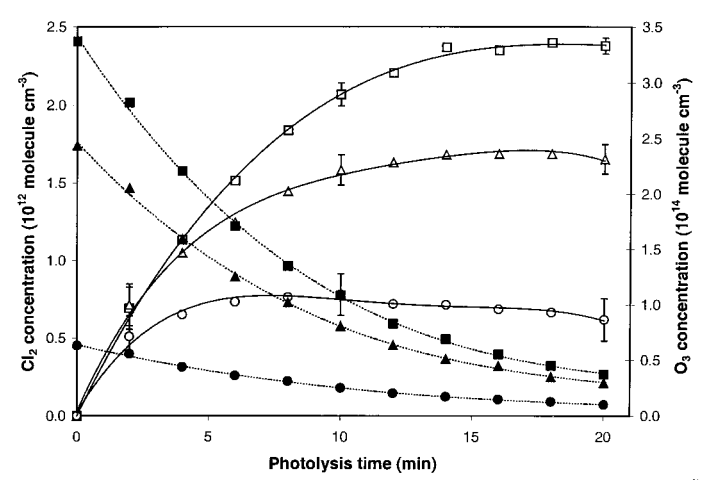
Model predictions with the use of conventional physical and chemical processes for the experiment with an initial O3 concentration of 2.4×10^{14} molecule cm⁻³ are shown in Fig. 2. The predicted Cl₂ concentrations are three orders of magnitude smaller than observed because of the initially neutral pH of the particles. As a result, the generation of chlorine atoms from the HOCl- intermediate via reaction 6 with H⁺ is slow relative to the rapid reverse of reaction 5 of HOCl- back to Cl- and OH, and the subsequent production of Cl2 via reactions 7 through 9 is small. To confirm the effects of acid on the predicted Cl, formation, we performed model runs in which a constant pH of either 3.5 or 4.0 was assumed. As seen in Fig. 2, the predicted initial rate of formation of Cl₂ at a pH of 4.0 is smaller than observed because of the second-order kinetics for the self-reaction 8 of Cl₂ in the bulk, and the predicted peak concentration was too small by a factor of 2. Although Cl₂ is produced more rapidly at a pH of 3.5, the peak concentrations are predicted at later times and are much larger than those measured experimentally. In addition, there is no known source of acid in the experimental system, which would provide a pH of 4.0 or less.

In short, conventional chemical and physical processes involving transport of gases to the particle surface, mass accommodation, diffusion, and known reactions in the bulk aqueous-phase of the particles, do not explain the experimental observations.

Molecular dynamics simulations. The solvation of NaCl and the nature of ion pairs in clusters and in concentrated bulk solutions have been explored theoretically (19-21). There is evidence that in aqueous solutions of inorganic salts, the large and polarizable anions are more readily available at the surface than the small nonpolarizable cations. This effect is present at the surfaces of both bulk solutions and finitesize molecular clusters. For example, a negative surface potential has been measured for NaCl solutions (22) and attributed in part to enhanced chloride ion concentrations near the surface. Theoretical studies report that in clusters of hundreds of water molecules, Cl- can be moved within several molecular layers of the surface before the free energy starts to increase significantly, whereas the free energy for Na+ increases continuously from the center of the cluster to the surface (23). Molecular dynamics simulations of Na⁺(H₂O)_n and Cl⁻(H₂O)_n (n = 4 to 14) clusters show that full ion solvation occurs in the former case, whereas surface solvation dominates for the chloride anion (24).

To understand the nature of the interface of microbrine droplets with which OH and

Fig. 1. Typical decay of O₃ and formation of Cl₂ as a function of time during the photolysis at 254 nm of a mixture of O₃ and deliquesced NaCl particles in air at 82% RH and 297 K. Conditions in the three experiments were as follows: (\blacksquare) $O_3 = 3.4 \times$ 10¹⁴ molecule cm⁻³, 1.9×10^{5} particle cm⁻³ with a count median diameter of 224 nm, geometric standard deviation $\sigma = 1.93$, surface area 6.1×10^{10} nm² cm⁻³, and volume

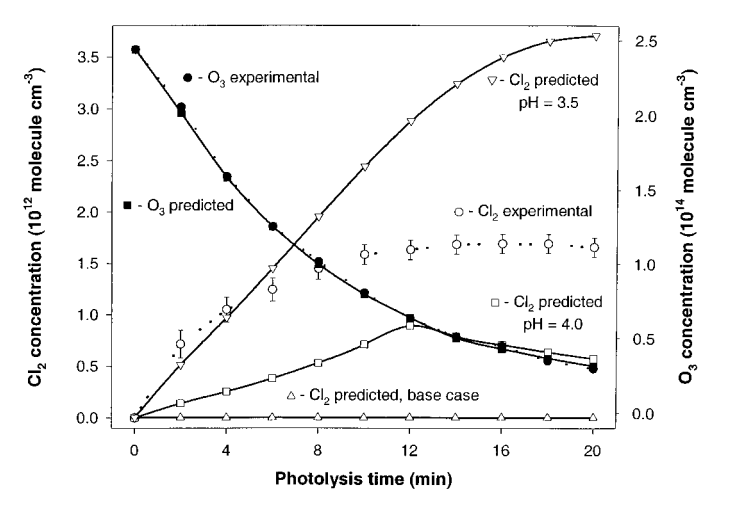


This volume of the properties of the state of the state

Table 1. Gas- and aqueous-phase species included in the computational model.

Species group	Aqueous phase	Gas phase
Oxygen- hydrogen	O(³ P), O ₂ , O ₃ , H ⁺ /OH ⁻ , OH/O ⁻ , HO ₂ /O ₂ ⁻ , H ₂ O ₂ /HO ₂ ⁻ , HO ₃ , O ₃ ⁻	O(¹D), O(³P), O ₂ , O ₃ , H ₂ O, OH, HO ₂ , H ₂ O ₂
Chlorine	Cl, Cl ₂ , Cl ₂ ⁻ , HCl/Cl ⁻ , HOCl/ClO ⁻ , HOCl ⁻ , ClO, ClO ₂ , ClO ₃ ⁻ , Cl ₂ O ₂	Cl, Cl ₂ , HCl, HOCl, ClO, OClO, ClOO, Cl ₂ O ₂
Carbonate and other	CO ₂ ·H̄ ₂ O/HCO ₃ ⁻ /CO ₃ ²⁻ , HCO ₃ /CO ₃ ⁻ , Na ⁺	CO ₂

Fig. 2. Experimental data and model-predicted O₃ decay and Cl₃ formation for the experiment in Fig. 1 in which $O_3 = 2.4 \times$ 10¹⁴ molecule cm⁻³. For this experiment, conventional gas-particle transport and chemical processes in the gas and bulk aqueous phases (base case) were used without fixing the pH or by assuming a constant pH $(= -\log a_{H+})$ of either 4.0 (\square) or 3.5 (∇). Experimental data are shown by ●, O₂ and ○,



other reactant gases in this system interact, we performed a series of molecular dynamics simulations of microbrines of different sizes, consistently keeping the NaCl concentration at the bulk saturation value. We investigated clusters ranging from NaCl(H₂O)_o to Na₃₂Cl₃₂(H₂O)₂₈₈, and with the use of twodimensional (2D) periodic boundary conditions, an "infinite" open surface (actually a double surface) with the unit cell formed by Na₉₆Cl₉₆(H₂O)₈₆₄. Two potential models, one nonpolarizable (25) and one explicitly including the polarizabilities of water and ions (26), were compared. Standard Lennard-Jones parameters for the ions were used in both cases (27). All interactions have been included for cluster studies, whereas for the slab with an open surface, an interaction cutoff of 12 Å was applied and long-range interactions were accounted for with the particle-mesh Ewald method (28). Simulations were run for 500 ps after a sufficiently long equilibration period of 250 ps. The slab with a flat surface mimics the atmospheric microbrines with typical diameters of 200 nm better than the small clusters with hundreds of atoms do. We therefore report our results primarily on the basis of slab simulations.

Figure 3 depicts a snapshot from the molecular dynamics run showing a typical arrangement of the open surface of the slab. The corrugated surface contains water molecules (red and white balls) and a large number of chloride ions (yellow balls). Sodium ions (green balls) are almost missing from the surface. This happens because the small sodium cations fit well into the hydrogen-bonded water structure and therefore are fully solvated, whereas the chloride anions are too large and, as a consequence, are to a great extent pushed toward the surface of the system. This effect is also present consistently in finite size clusters of different sizes and seems to be pertinent to concentrated solutions of ions of different relative sizes in a polar medium.

The degree of surface exposure of the ions will strongly influence their surface reactivity toward gas phase reactants. To quantify this, we have applied a standard procedure of evaluating the accessible surface area of the two ions by rolling a particle of the size of the OH radical (radius of 1.7Å) over the surface of the slab at each time step of the dynamical run. The relative accessible areas (with respect to the total surface) of the Na+ and Clions from both the polarizable and nonpolarizable potential model are shown in Fig. 4. Both models qualitatively predict that although the Na+ ions are fully solvated and almost absent at the surface, the Cl- ions occupy a significant part of the surface of the slab. Quantitatively, the nonpolarizable and polarizable models predict that 3.3 and 11.9% of the surface is covered by chloride ions, respectively, whereas both models predict that the sodium cations occupy less than 0.2% of the surface.

The dramatic difference between the solvation of the two ions is not only due to their different sizes but also to a much larger polarizability of Cl⁻, which also explains the quantitative discrepancy between the two potential models. Comparison of previous molecular dynamics simulations of clusters with only one type of ion to experimental measurements (24) as well as our preliminary first-principle molecular dynamics with a density functional interaction model (29) for Cl⁻(H₂O)₆ indicates that the polarizable model is the more accurate one (24). Assuming that about 12% of the surface is covered by Cl⁻ and that the ratio between the number of NaCl and water species is 1:9, the chloride ion actually has more surface exposed than an average water molecule.

Our simulations confirm that chloride anions, unlike the sodium cations, occupy a significant fraction of the microbrine surface. This is a robust effect that qualitatively depends neither on the size of the microbrines nor, within relatively broad margins, on temperature. Two different potential models coherently predict this behavior, and the more accurate model also predicts more surface chloride anions.

Finally, in agreement with experimental findings (4, 5), we found that chloride ions strongly attract surrounding reactive particles. Using practically converged quantum chemical calculations [coupled clusters with single and double excitations and perturbative triples with an augmented correlation corrected Dunning polarization double-zeta basis set and with correction for the basis set superposition error (30)], we have evaluated affinities of Cl⁻ toward the OH radical and compared them to those of the water molecule. The complexation energy rises dramatically from 4.9 to 16.9 kcal mol⁻¹ from H₂O to Cl⁻, suggesting that chloride anions can actually enhance the scavenging of reactive species from the atmosphere with which they then undergo chemical reactions.

Integration of experiments and simulations. The combination of experimental observations, computer kinetic modeling with the use of only gas- and bulk aqueous-phase chemistry, molecular dynamics simulations, and quantum chemical calculations strongly suggests that chemistry at the interface is responsible for the observed production of Cl_2 . We propose that the key step in the generation of Cl_2 in the chamber is the reaction of OH with chloride at the interface

$$OH_{(g)} + Cl^{-}_{(interface)} \rightarrow (OH...Cl^{-})_{interface}$$
(12)

which then reacts further, ultimately forming Cl₂. The structure of the bound complex between OH and Cl⁻ is likely to involve interaction between the hydrogen of the OH and the chloride ion. Such an intermediate has been

observed in the gas phase upon electron impact on a mixture of HCl and $\rm N_2O$ (31) and has been explored experimentally and theoretically in electron spin resistance studies of the low-temperature reaction of OH with chloride ions (32). We assume here that the OH...Cl $^-$ intermediate undergoes a self-reaction in a manner similar to that of another chlorine-containing radical anion, Cl $_2$ $^-$ (reaction 8)

$$(OH...Cl^{-})_{interface} + (OH...Cl^{-})_{interface}$$

 $\rightarrow Cl_{2} + 2OH^{-}$ (13)

Other potential mechanisms that could generate Cl₂ were also considered (*33*); this one is presented because it provides good overall fits to the experimental data and is thermodynamically and kinetically feasible.

Figure 5 shows schematically the overall chemistry and mass transfer processes considered in this model. In contrast to the mechanism represented by reactions 5 through 9, the interfacial reaction proposed here does not require an acid for Cl2 production. Instead, OH- is produced. Cl2 is known to react rapidly with OH⁻ so that if the droplets become highly alkaline, Cl2 is taken up into the aqueous phase and hydrolyzed, which results in much smaller predicted gas-phase concentrations of Cl₂. However, the particles in the experiment are buffered by small amounts of gaseous CO2 [~13 parts per million (ppm)] that are present from the CaCO₃ drying agent in the particle diffusion dryer. The computer kinetic model includes the uptake of CO₂ and the aqueous-phase chemistry of carbonate and bicarbonate. As a result of these buffering reactions, the predicted pH in the droplets reaches the range of 8 to 9.

Production of Cl₂ is modeled under the assumption that a three-step process occurs at the interface, in addition to conventional transport

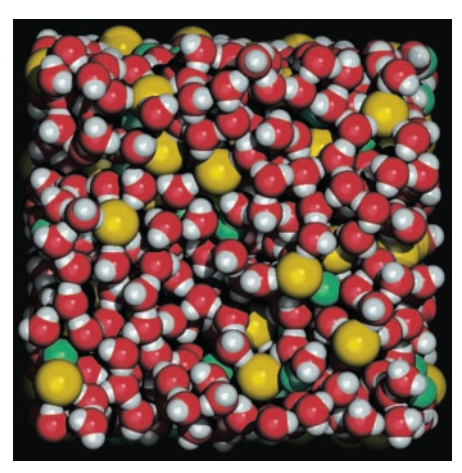


Fig. 3. Snapshot of molecular dynamics predictions of typical open surface of a slab consisting of 96 NaCl molecules and 864 water molecules. The large yellow balls are Cl^- ions, the smaller green balls Na^+ , and the red and white balls are water molecules.

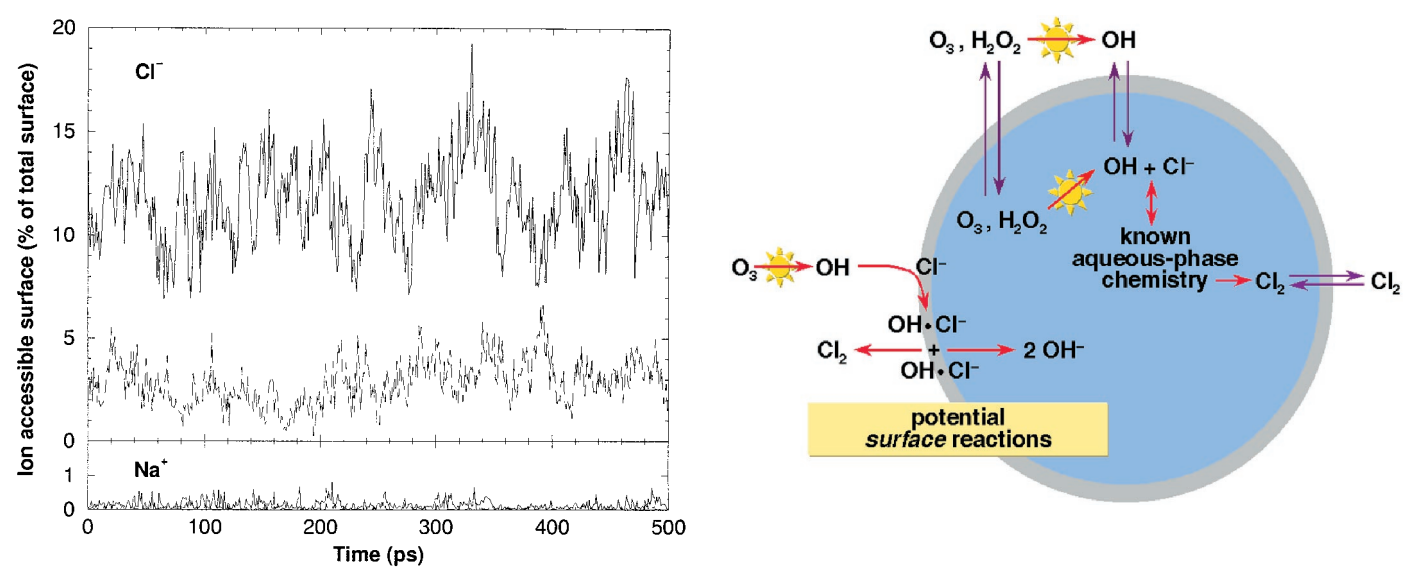
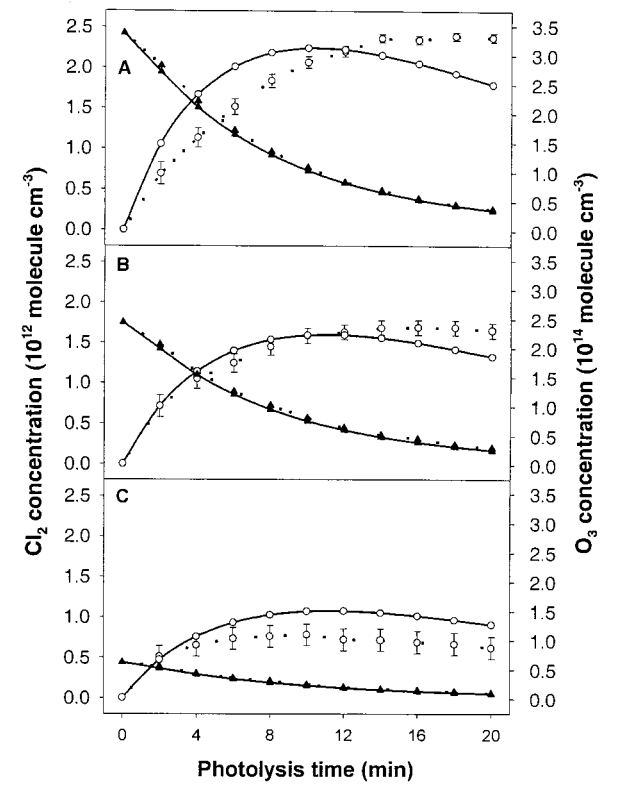


Fig. 4 (left). Predicted relative surface-accessible areas for Na⁺ and Cl⁻ with the use of the polarizable (solid lines) and nonpolarizable (broken lines) potential models, respectively. Fig. 5 (right). Schematic diagram of kinetic model of gas particle system.

Fig. 6. Model-predicted Cl₂ formation (\circ) and O_3 loss (\triangle) when the interface reactions are included in computational kinetic model. Experimental data, dotted lines; model predictions, solid lines. The model takes into account both dilution, which occurs during the experiment while sampling into the API-MS to measure Cl₂, and small losses of Cl₂ at the chamber walls and from photolysis, which were determined independently with authentic samples of Cl₂. (A through C) correspond to three experiments with different initial O_3 concentrations as in Fig. 1.



into and reaction in the bulk aqueous phase of the particles. The rate of reaction 12 is set equal to the number of OH-particle surface collisions per second, multiplied by the ratio of the chloride ion to water concentrations, and scaled by a factor of 1.6 for the relative areas of a chloride ion and water, consistent with the polarizable molecular dynamics results that predict 12% of the surface is covered by chloride ions. A time-dependent scaling factor is also included to account for the fact that a chloride ion already existing as a bound (OH...Cl)⁻ complex would

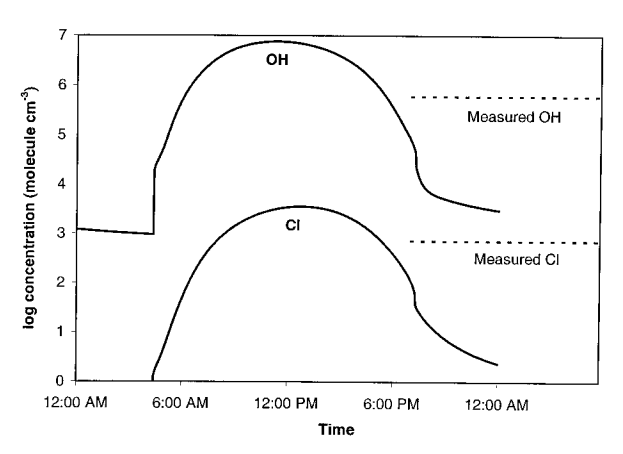
not react with an incoming gas phase OH. This approach is applicable when the collisions are random with all surface sites without a strong propensity for hitting a chloride ion. This model is conservative because OH collisions may result in sticking to the surface with longer residence times, which will give a higher reactivity than the estimate based simply on collision rates. The rate constant for reaction 13 is assumed to be the same as that for the self-reaction of Cl_2^- , $1.8 \times 10^9 \, \text{l mol}^{-1} \, \text{s}^{-1}$ (34). The (OH...Cl)⁻ intermediate was assumed to

exist in a volume corresponding to a 1-nm shell on the outside of the particle. In addition to its self-reaction, it is also assumed to decompose back to reactants with a rate constant of 1×10^4 s⁻¹, which was chosen to provide the best fit to the experimental observations. However, similar fits can also be obtained with smaller decomposition rate constants for OH...Cl⁻ along with smaller values of the probability for reaction 12 forming OH...Cl⁻.

Figure 6 shows the model-predicted concentrations of O₂ and Cl₂ when the surface reactions are included, along with the full suite of gas- and liquid-phase chemistry and mass transfer processes for the bulk phases described above for the three different initial ozone concentrations (Fig. 1). The model predictions are much more consistent with both the time-dependent and the peak levels of Cl2 observed experimentally than the base case, which uses only known gas and bulk aqueous-phase chemistry, or the predictions that assume a constant pH of 3.5 to 4.0 (Fig. 2). Indeed, the predicted Cl₂ concentrations are always within 50% of those observed experimentally, and the time profiles are in qualitative agreement despite the uncertainties in the fates of (OH....Cl)- at the interface and the simple reaction scheme used.

Application to atmospheric marine boundary layer. Computational kinetic studies were also performed for conditions more representative of the marine boundary layer (35, 36) using the mechanism that includes the surface reactions. Salt particles were assumed to be present with a number concentration of 10 cm^{-3} and a diameter of $2 \mu \text{m}$. Figure 7 shows the model predictions for Cl atoms and OH radicals for a 24-hour diurnal cycle for remote marine boundary layer conditions. The reported diurnal averages for OH and Cl (35) over 24 days are also shown,

Fig. 7. Model-predicted Cl atom and OH radical concentrations over a 24-hour period under remote boundary layer conditions. Initially, concentrations of ethane, propane, dimethyl sulfide, NO and O₃ are 370 parts per trillion (ppt), 11 ppt, 200 ppt, 3 ppt, and 25 parts per billion, respectively, consistent with measured values in the Southern Ocean (*35*, 40). Monodisperse salt particles are present with a number concentration of 10 cm⁻³ and a diameter of 2 μm.



which include light and dark periods as well as times when sea salt particles had been washed out by storms. Given the different time scales and conditions involved in the model and measurements and that the model does not include transport or emissions, the model predictions and the field results are in excellent agreement. The pH of the particles was predicted to have dropped to ~4 after 24 hours, so acid-catalyzed bulk aqueous phase chemistry also contributes to the production of chlorine atoms (\sim 60% of the total). Model calculations were also carried out for a Lagrangian field experiment over the North Atlantic Ocean (36). In this case, the model predicts a chlorine atom concentration of 3.7×10^4 atoms cm⁻³ at noon, compared to a measured value of 6.5×10^4 atoms cm⁻³ for a 2-hour period leading up to local noon, again in good agreement given the uncertainties in both the model and the measurements. Under these more polluted conditions, the pH of the particles is predicted to fall to ~ 3.2 after 2 hours, so that bulk aqueous phase chemistry predominates in the chlorine atom production (80% of the total). Under these atmospheric conditions, the major source of Cl₂ from the bulk, aqueous phase chemistry is the acid-catalyzed reaction of HOCl with Cl⁻. In the absence of the interface reaction, chlorine atoms are generated primarily from OH + HCl, ultimately forming gas phase HOCl that is taken up into the aqueous phase. Clearly, the surface reactions will be most important at pH values above about 4.

Given the ubiquitous occurrence of sea salt particles in the marine boundary layer and the potential importance of their reactions in midlatitudes and in the Arctic, it is critical that such chemistry at interfaces be taken into account in field, laboratory, and tropospheric modeling studies. Furthermore, there is an urgent need for the development and application of experimental methods of detection of such radical surface species. Molecular dynamics simulations suggest that the availability of anions at the interface is not unique to chloride. If this availability is determined largely by the size and polarizability of the anion, then bromide should be

even more evident at the surface of concentrated sea salt particles, enhancing its chemistry relative to chloride as has been observed in a variety of laboratory (37) and field (38) studies. Another factor in this enhancement may be that Br-, unlike Cl-, is oxidized by O3 at room temperature (39). Furthermore, quantum chemical calculations have shown that the complexation energy of O₂ and Cl⁻ is larger than O₂ and H₂O (5.5 versus 1.6 kcal) and might be expected to be larger for O₂ and Br⁻ as well. Finally, the possible role of anions such as sulfate and nitrate that are considered unreactive in the atmosphere in increasing the scavenging of gases and, hence, altering their heterogeneous chemistry, also needs to be considered in assessing the contribution of highly concentrated inorganic salt particles to chemistry in the atmosphere.

References and Notes

- B. J. Finlayson-Pitts and J. N. Pitts Jr., Chemistry of the Upper and Lower Atmosphere: Theory, Experiments and Applications (Academic Press, San Diego, CA, 2000), and references therein.
- J. T. Jayne, P. Davidovits, D. R. Worsnop, M. S. Zahniser, C. E. Kolb, *J. Phys. Chem.* **94**, 6041 (1990).
 D. J. Donaldson, J. A. Guest, M. C. Goh, *J. Phys. Chem.*
- D. J. Donaldson, J. A. Guest, M. C. Goh, J. Phys. Chem. 99, 9313 (1995).
- 4. J. H. Hu et al., J. Phys. Chem. 99, 8768 (1995).
- 5. L. Magi et al., J. Phys. Chem. A **101**, 4943 (1997).
- 6. D. R. Hanson, J. Phys. Chem. B 101, 4998 (1997).
- W. Behnke, V. Scheer, C. Zetzsch, in Naturally Produced Organohalogens, (Kluwer, Dordrecht, Netherlands, 1995), pp. 375–384.
- K. W. Oum, M. J. Lakin, D. O. DeHaan, T. Brauers, B. J. Finlayson-Pitts, Science 279, 74 (1998).
- W. L. Chameides and A. W. Stelson, J. Geophys. Res. 97, 20565 (1992).
- R. Sander and P. J. Crutzen, J. Geophys. Res. 101, 9121 (1996).
- D. R. Kester, I. W. Duedell, D. N. Conners, R. M. Pytkowicz, Limnol. Oceanogr. 12, 176 (1967).
- 12. The apparatus is described in detail by D. O. De Haan et al. [Int. Rev. Phys. Chem. 18, 345 (1999)]. Briefly, it consists of a 561-l aluminum and stainless steel chamber that is coated with halocarbon wax (Halocarbon Products Series 1500, River Edge, NJ) to minimize the reactivity of the surfaces. It has White cell optics for UV-visible absorption spectrometry used to measure O₃ and FTIR for O₃, CO₂, and other infrared-absorbing gases. For both optical systems, the base path is 2 m; a total path of 52.5 m was used in these studies. The Cl₂ is measured with API-MS in the negative ion mode using the peaks at mass to electron ratio (m/e) = 70, 72, and 74.
- I. N. Tang, A. C. Tridico, K. H. Fung, J. Geophys. Res. 102, 23269 (1997).

- 14. D. Dabdub and J. H. Seinfeld, Parallel Computing 22, 111 (1996).
- 15. These species include HO_2 , H_2O_2 , OH, O_3 , O_2 , HCl, HOCl, Cl_2 , OClO, and CO_2 . The rate of transport due to gas-phase diffusion and mass transport at the droplet interface for a given species is evaluated via a mass transfer coefficient $k_{\rm mt}$ calculated as

$$k_{\rm mt} = \left[\frac{R_{\rm p}^2}{3D_{\rm g}} + \frac{4R_{\rm p}}{3\bar{c}\alpha}\right]^{-1}$$

where R_p is the droplet radius taken to be the radius of average surface area in the experiments, D_g is the gas-phase diffusivity, \bar{c} is the mean molecular speed, and α is the mass accommodation coefficient. The effect of diffusion on the overall rate of reaction of species in the bulk of the droplet is determined for species that are transported actively between the gas and aqueous phase and their hydrolysis and/or dissociation products. The average bulk concentration for these species is determined by solving a system of tightly coupled nonlinear equations emerging from solutions to the steady state aqueous-phase diffusion equation. In these equations, we consider both loss and production terms within the droplet that are calculated from the average bulk concentration of other species. Specifically, the average bulk concentration for species "j" is described as

$$\begin{split} \langle C_j \rangle &= Q C_j^* + \{1-Q\} \, \frac{P_j}{k_{\mathrm{L},j}} \\ \text{where } Q &= 3 \bigg(\frac{\coth q_j}{q_j} - \frac{1}{q_j^2} \bigg) \, \text{and} \, q_j = \, R_\mathrm{p} \bigg(\frac{k_{\mathrm{L},j}}{D_{\mathrm{aq},j}} \bigg)^{1/2} \end{split}$$

 $D_{\rm aq}$ represents the aqueous-phase diffusivity, $k_{\rm L}$ is the effective overall first-order rate constant for aqueous-phase losses, and P is the overall production term.

- S. E. Schwartz, in Chemistry of Multiphasic Atmospheric Systems, NATO ASI Series, W. Jaeschke, Ed. (Springer-Verlag, New York, 1986), vol. G6, pp. 415– 471.
- K. S. Pitzer, in Activity Coefficients in Electrolyte Solutions, K.S. Pitzer, Ed. (CRC Press, Boca Raton, FL, ed. 2, 1991), pp. 75–153.
- V. L. Snoeyink and D. Jenkins, Water Chemistry (Wiley, New York, 1980).
- 19. P. Jungwirth, J. Phys. Chem. A **104**, 145 (2000).
- L. Degrève and F. L. B. da Silva, J. Chem. Phys. 110, 3070 (1999).
- C. P. Petersen and M. S. Gordon, J. Phys. Chem. A 103, 4162 (1999).
- N. L. Jarvis and M. A. Scheiman, J. Phys. Chem. 72, 74 (1968).
- M. A. Wilson and A. Porohille, J. Chem. Phys. 95, 6005 (1991).
- L. Perera and M. L. Berkowitz, J. Chem. Phys. 95, 1954 (1991).
- 25. G. J. Martyna et al., PINY-MD program, unpublished.
- D. A. Pearlman et al., Comput. Phys. Commun. 91, 1 (1995).
- 27. A. D. MacKerell Jr et al., J. Phys. Chem B. **102**, 3586 (1998)
- U. Essmann, L. Perera, M. L. Berkowitz, T. Darden, L. G. Pedersen, *Chem. Phys.* **103**, 8577 (1995).
- L. M. Ramaniah, M. Bernasconi, M. Parrinello, J. Chem. Phys. 109, 6839 (1998).
- M. J. Frisch et al., Gaussian98 computer program (Gaussian, Pittsburgh, PA, 1998).
- M. J. Davis, H. Koizumi, G. C. Schatz, S. E. Bradforth,
 D. M. Neumark, J. Chem. Phys. 101, 4708 (1994).
- M. D. Sevilla, S. Summerfield, I. Eliezer, J. Rak, M. C. R. Symons, J. Phys. Chem. A 101, 2910 (1997).
- 3. Other mechanisms considered are as follows: (i) the reaction of OH with Cl⁻ to give HOCl⁻, which diffuses into the bulk and reacts but does not generate significant amounts of Cl₂; (ii) electron transfer from OH...Cl⁻ to form HOCl, which then reacts with OH...Cl⁻. This gives good fits to the experimental observations but is sufficiently endothermic that it does not appear to be a viable mechanism. (iii) Reaction of OH...Cl⁻ with Cl⁻ to form Cl₂⁻, which generates Cl₂ by photodetachment. This mechanism predicted a significant induction time for gaseous Cl₂ formation, which is inconsistent with the experimental observations. (iv) Decomposition of the bulk

aqueous phase HOCl $^-$ to generate, ClO $^{2-}$ + H $^+$, proposed as a possibility by Jayson *et al.* [*J. Chem. Soc., Faraday Trans. I.* **69**, 1597 (1973)]. This acidifies the droplet and generates Cl $_2$ via reactions 6 through 9. Unless HOCl $^-$ is assumed to be an infinitely strong acid, this does not generate significant Cl $_2$ concentrations; (v) the reaction of the surface (OH... Cl $^-$)_{interface} with Cl $^-$ to generate Cl $_2$ $^-$, which then self-reacts in the surface film to form Cl $_2$. This can also match the experimental data reasonably well if it is assumed that Cl $_2$ $^-$ is "anchored" to the surface and does not diffuse into the bulk aqueous phase. Preliminary molecular dynamics

- calculations do indeed indicate that ${\rm Cl_2}^-$ is locked to the interface of the concentrated salt microaerosols.
- 34. H. W. Jacobi, F. Wicktor, H. Herrmann, R. Zellner, *Int. J. Chem. Kinet.* **31**, 169 (1999).
- 35. O. W. Wingenter *et al.*, *J. Geophys. Res.* **104**, 21819 (1999).
- 36. O. W. Wingenter et al., J. Geophys. Res. **101**, 4331 (1996).
- See for example, K. W. Oum, M. J. Lakin, B. J. Finlayson-Pitts, Geophys. Res. Lett. 25, 3923 (1998).
- 38. L. Barrie and U. Platt, Tellus 49B, 450 (1997).
- 39. H. Taube, J. Am. Chem. Soc. 64, 2468 (1942).

Impaired Nociception and Pain Sensation in Mice Lacking the Capsaicin Receptor

M. J. Caterina, 1* A. Leffler, 3 A. B. Malmberg, 2† W. J. Martin, 2‡
J. Trafton, 2 K. R. Petersen-Zeitz, 2 M. Koltzenburg, 3
A. I. Basbaum, 2 D. Julius 18

The capsaicin (vanilloid) receptor VR1 is a cation channel expressed by primary sensory neurons of the "pain" pathway. Heterologously expressed VR1 can be activated by vanilloid compounds, protons, or heat (>43°C), but whether this channel contributes to chemical or thermal sensitivity in vivo is not known. Here, we demonstrate that sensory neurons from mice lacking VR1 are severely deficient in their responses to each of these noxious stimuli. VR1^{-/-} mice showed normal responses to noxious mechanical stimuli but exhibited no vanilloid-evoked pain behavior, were impaired in the detection of painful heat, and showed little thermal hypersensitivity in the setting of inflammation. Thus, VR1 is essential for selective modalities of pain sensation and for tissue injury—induced thermal hyperalgesia.

Pain-producing stimuli are detected by specialized primary afferent neurons called nociceptors. These remarkable cells respond to a broad spectrum of physical (heat, cold, and pressure) or chemical (acid, irritants, and inflammatory mediators) stimuli but do so only at stimulus intensities capable of causing tissue damage (1). Little is known about the molecules that account for the specialized properties of nociceptors. One noxious stimulus for which a candidate transduction protein has been described is capsaicin, the lipophillic vanilloid compound that renders "hot" chili peppers pungent (2). Capsaicin and structurally related molecules, such as the ultrapotent irritant resiniferatoxin, bind to specific vanilloid receptors on the peripheral terminals of nociceptive neurons (3, 4). Receptor occupancy triggers cation influx, action potential firing, and the consequent burning sensation associated with spicy food (2). We recently identified a cDNA encoding a vanilloid-activated cation channel (VR1) (5) that is selectively expressed by small- to medium-diameter neurons within dorsal root, trigeminal, and nodose sensory ganglia (5–7). When expressed heterologously in transfected mammalian cells or frog oocytes, VR1 can also be activated by protons (extracellular pH < 6) or noxious heat (>43°C) (5, 7), both of which excite nociceptors and evoke pain in humans or pain-related behaviors in animals (8–12).

Although these in vitro studies suggest that VR1 serves as a transducer of noxious thermal and chemical stimuli in vivo, this hypothesis is controversial on several fronts. First, multiple vanilloid receptor subtypes have been proposed to exist (13, 14), and thus the extent to which VR1 is required for capsaicin-evoked nociceptive responses is unknown. Second, acidosis produces an array of electrophysiological responses in sensory neurons (15, 16), and extracellular protons may interact with targets other than vanilloid receptors on these cells, most notably acid-sensing ion channels (ASICs) of the degenerin family (17–19). Thus, the relative contributions of VR1 and

- F. B. Griffiths, T. S. Bates, P. K. Quinn, L. A. Clementson and J. S. Parslow, J. Geophys. Res. 104, 21649 (1999).
- 41. The authors are grateful to NSF; the Department of Energy; the UCI Council on Research, Computing, and Library Resources; and NATO for support of this work. E.K. thanks the Organization of American States for a PRA Fellowship. We thank J. N. Pitts Jr., J. C. Hemminger, R. E. Huie, D. Margerum, R. Sander, and P. Davidovits for helpful discussions and E. Chapman, C. Berkowitz, and C. W. Spicer for providing some of the gas-phase model.
 - 29 November 1999; accepted 11 February 2000

ASICs to proton-evoked nociceptor excitability and pain are not understood. Third, the link between vanilloid receptors and thermal nociception is tentative because some, but not all, biophysical and pharmacological properties of VR1 resemble those of native heat-evoked responses in sensory neurons (5, 7, 20–25). Finally, capsaicin- and heat-evoked single channel responses do not always cosegregate in membrane patches from cultured rat sensory neurons (25). These discrepancies raise the possibility that VR1 is not involved in thermal nociception and pain in the whole animal.

Here we adopt a genetic strategy to determine whether VR1 contributes to activation of the "pain" pathway by noxious chemical or thermal stimuli. Using a variety of cellular and behavioral assays, we show that disruption of the VR1 gene in mice eliminates capsaicin and resiniferatoxin sensitivity, demonstrating that VR1 is essential for mediating the actions of these compounds in vivo. Sensory neurons and primary afferent fibers from these mice also show a marked reduction in proton (pH 5) sensitivity in vitro, supporting the notion that VR1 contributes to acid-evoked nociception. We also show that the incidence of noxious heat-evoked currents of the moderate-threshold (>43°C) class is greatly reduced in cultured sensory neurons or sensory nerve fibers from VR1 mutant mice. VR1null animals exhibit marked, but restricted deficits in their behavioral responses to noxious thermal stimuli, proving that VR1 is essential for normal thermal nociception. Moreover, the existence of residual heatevoked responses in these animals demonstrates that thermal nociception is a heterogeneous process involving multiple transduction mechanisms.

Sensory ganglion development. The mouse VR1 gene was disrupted by deleting an exon encoding part of the fifth and all of the sixth putative transmembrane domains of the channel, together with the intervening pore-loop region (Fig. 1A) (26). The gene is located on a somatic chromosome (11B3) (27), and matings between VR1 heterozygous mice produced offspring with expected Mendelian distributions of gender and genotype (Fig. 1B). Dorsal root ganglia (DRG) from null mutant mice lacked detectable VR1 transcripts (Fig. 1C). VR1^{-/-} mice were viable, fertile, and largely

¹Department of Cellular and Molecular Pharmacology, ²Departments of Anatomy and Physiology and the W. M. Keck Center for Neuroscience, University of California, San Francisco, San Francisco, CA 94143–0450, USA. ³Department of Neurology, University of Würzburg, D-97080 Würzburg, Germany.

^{*}Present address: Department of Biological Chemistry, Johns Hopkins University School of Medicine, Baltimore, MD 21205, USA.

[†]Present address: Neurobiology Unit, Roche Bioscience, Palo Alto, CA 94304–1397, USA.

[‡]Present address: Merck Research Laboratories, Rahway, NJ 07065, USA.

[§]To whom correspondence should be addressed. E-mail: julius@socrates.ucsf.edu